

MODELING OF THE ROLLING AND SLIDING CONTACT BETWEEN TWO ASPERITIES**PART II: HEMISPHERICAL SLIDING CONTACT****V. Boucly (LaMCoS – UMR CNRS
5514, INSA Lyon, France)****D. Nélias (LaMCoS – UMR CNRS
5514, INSA Lyon, France)****I. Green (Georgia Institute of
Technology, Atlanta, USA)****ABSTRACT**

The first part of the paper proposed a semi-analytical method for the tridimensional thermal-elastic-plastic contact between two hemispherical asperities. The algorithm has been described for both the load-driven (ld) and the displacement-driven (dd) formulations, and validated through a nano-indentation test simulation. The way to consider rolling and sliding motion of the contacting bodies consists of solving the elastic-plastic contact at each time step while upgrading the geometries as well as the hardening state along the moving directions. The derivations concerning the interference calculation at each step of the sliding process are then shown, and an application to the tugging between two spherical asperities in simple sliding (dd formulation) is made. The way to project the forces in the global reference is outlined, considering the macro-projection due to the angle between the plane of contact and the sliding direction, and the micro-projection due to the pile-up induced by the permanent deformation of the bodies due to their relative motion. Finally a load ratio is introduced and results are qualitatively compared to a two-dimensional FEM analysis presented elsewhere.

INTRODUCTION

This paper deals with the rolling and sliding contact between two asperities. Jacq et al. [1] first introduced a Semi-Analytical Method (SAM) to study the rolling of a normal load over a surface defect. Following the same method, Liu et al. [2] built a model that deals with normal thermal-elastic contact calculation. In combining these two formulations, Boucly et al. [3] developed a new code that allows studying thermal-elastic-plastic (TEP) contacts. All these formulation are based on the use of numerical accelerating techniques, making transient analysis affordable including when a fine mesh is required. Most commonly used numerical techniques are the Conjugate Gradient (CG) method first introduced by Nogi and Kato [4],

later used by Polonsky and Keer [5], the Multi Level Multi Summation (MLMS) technique first implemented by Lubrecht and Ioannides [6], and the Discrete Convolution and Fast Fourier Transform (DC-FFT) used by Nogi and Kato [4] and later by Liu et al. [7] combined to the CGM. The applications of this formulation are various, such as the determination of the micro-yield stress profile in a nitrided steel by nano-indentation [8], the rolling of a load on a smooth, dented or rough surface [1, 9], the vertical and tangential loading [10], the simulation of fretting wear [11], and the running-in or wear of initially smooth or rough surfaces [12].

This paper is focused on the simulation of asperities tugging in simple sliding motion. For that purpose the TEP contact model [3] was improved in several ways [13]. It should be pointed out that the displacement-driven (dd) formulation is well adapted to the localized contact between two opposite asperities since the load distribution between asperities for real rough surfaces is not known a priori.

Sliding contacts are present in many mechanical components. They are also observed in human joints, as pointed out by Chen et al. [14], where a 2D simulation has been performed using the Finite Element Method (FEM). This modeling is similar than the one used by Vijaywargiya and Green [15]. The later are the first researchers that uncoupled the effect of mechanical deformation and the effect of friction in sliding contacts. Previous researchers tried to model sliding contact, but they actually studied the effect of an increase in the friction coefficient on the contact between a sphere and a rigid flat [16, 17, 18] or between two spheres [19], the later showing extremely long execution times. Nosonovsky and Adams simulated the contact between two cylinders [20] whose surface is not smooth.

The current paper then focuses only on the mechanical deformation involved in sliding contact in order to uncouple the phenomenon. Compared to previous researcher's models, the

proposed method could be applied either to statistical or deterministic approaches, in order to study the rolling and sliding thermal-elastic-plastic contact between real 3D rough surfaces. It is to be noted that the bodies in contact can follow any hardening law, i.e. they are not restricted to be perfectly plastic.

NOMENCLATURE

(Thermal-)Elastic-Plastic contact

p = pressure, Pa
 α = interference, m
 u^r = residual displacement, m
 ε^p = plastic strain tensor, -

Elastic constants

ν = Poisson ration
 E = Young modulus, Pa
 E' = equivalent Young modulus, Pa

Geometry, sliding contact

R_1, R_2 = radius of body 1 and 2, respectively, m

R = equivalent radius, m

ω = global center separation, m

ω' = local center separation, m

(X, Z) = global reference

(x', z') = local reference

d_0 = initial distance before sliding, m

d = sliding distance, m

Δ = shifting distance, m

$\hat{\Delta}$ = corrected shifting distance, m

θ = angle of the plane of contact, rad

F_X, F_Y, F_Z = tangential loads and normal load,

respectively, N

F_X/F_Z = load ratio, -

θ_{px}, θ_{py} = pile-up angles, rad

S_y = yield strength, Pa

α_c = critical interference, m

P_c = critical load, N

U_c = critical potential (strain) energy, N.m

$C(v)$ = Critical yield stress coefficient, -

U = potential (strain) energy, N.m

MODELING OF THE ROLLING / SLIDING CONTACT BETWEEN TWO (THERMAL)-ELASTIC-PLASTIC ASPERITIES USING THE DD FORMULATION

The analysis of the contact between two asperities requires considering a relative velocity between the bearing surfaces. In addition when the tugging asperities bear only a small portion of the total load, it is clear that this transient contact will be better described by the dd formulation than by the ld one since both the subsequent localized normal and tangential loads will quickly change from zero to a maximum and then go back to zero (meaning no contact). A schematic view at the beginning of the collision is shown in Fig. 1 when one of the asperities is

being translated along the rolling/sliding direction relatively to the other one.

In the current incremental procedure, the normal contact is solved at every step, following the procedure described in [13]. The geometry, the hardening state as well as the plastic strains are updated at the end of each step for each Elastic-Plastic (EP) body. When the asperities are moving the geometry change includes the permanent deformation of the surface of the EP bodies. Special care to the effects of sliding will be given since it is a more complex problem than the pure rolling situation. Finally, some results on how both the normal and the tangential loads vary during a single tugging between two interfering asperities in rolling / sliding contact will be presented.

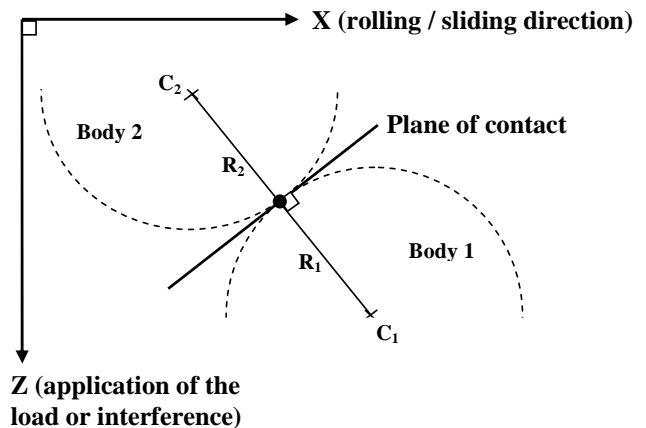


Fig. 1 – Schematic view of the tugging between two interfering asperities in rolling / sliding

Update of the geometry, hardening and plastic strains

The first step in transient contact calculation is to compute the static normal contact. If one of the bodies is considered elastic, then at the end of the first contact calculation, one has the situation presented Fig. 2a. For the next step, the residual displacement, the hardening state and the plastic strains are simply shifted from a value noted Δ and the new contact calculation can be processed, see Fig. 2b. As a general comment, this “updating” is only possible with the assumption that both bodies are considered as half spaces, to be coherent with the SAM used and its limitations, see [1] and [3].

If both bodies are considered elastic-plastic, the pure rolling and the rolling plus sliding situations should be differentiated. For the pure rolling case, starting from the initial configuration given Fig. 3a, the problem is very similar to the contact between an elastic body pressed against an elastic-plastic body, except that (i) the hardening state and the plastic strains are simply shifted for both bodies after each step; (ii) whereas the residual displacement is doubled, as seen Fig. 3b. The new contact calculation can then be processed.

For the (rolling plus) sliding contact the situation is more complicated. Starting from the initial configuration described in Fig. 4a, where the hardening state and the plastic strains are

simply shifted, it is clear that the residual displacement history should be considered individually for each surface, as it can be seen Fig. 4b.

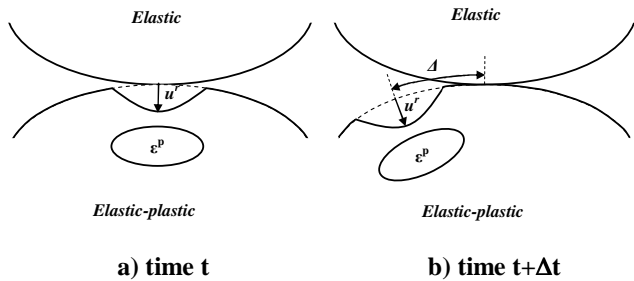


Fig. 2 – Updating at the end of the first loading step if one of the bodies is elastic.

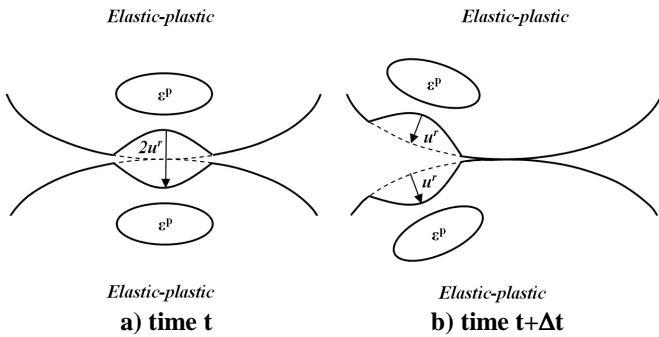


Fig. 3 – Updating at the end of the first loading step if both bodies are elastic-plastic. Case of pure rolling.

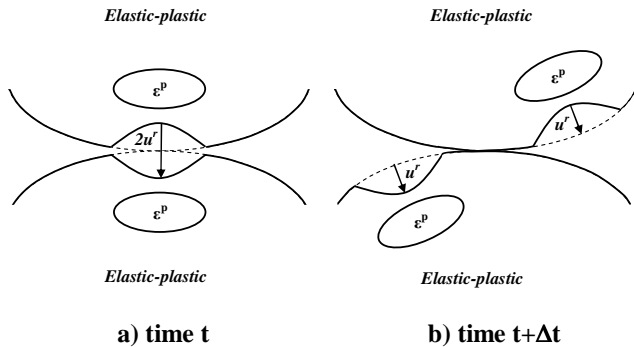


Fig. 4 – Updating at the end of the first loading step if both bodies are elastic-plastic. Case of rolling plus sliding contact.

Calculation of the local interference

A global and a local references will be considered to model the transient contact during tugging, as shown Fig. 5. The local referential (x', z') is linked to the plane of contact. A global interference is first applied in the global reference, by maintaining the global center separation, ω , along the Z-direction constant during tugging. Then one of the bodies is shifted of d in the perpendicular direction (X-direction). As a

consequence, the local center separation, ω' , along the z' -direction of the local reference will be different at every step of the computation.

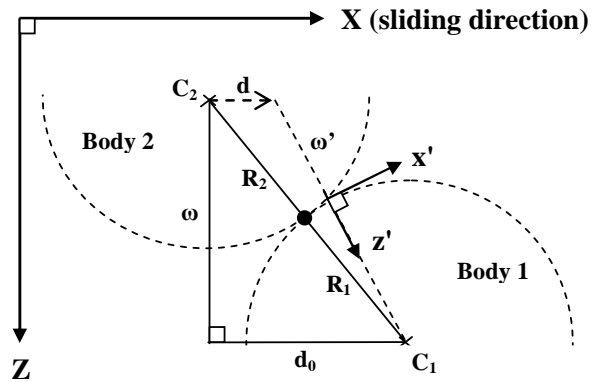


Fig. 5 – Definition of the Global (X,Z) and Local (x',z') references. Here the initial state when asperities start to tug each other is represented.

The initial state is considered first, see Fig. 5. The global center separation ω is applied in Z-direction, and the two bodies are put in contact. If d_0 is the initial distance between the two centers C_1 and C_2 in X-direction, then the local center separation ω' in z' -direction can be expressed as a function of the global center separation ω , d_0 and d , the latter being the sliding distance in X-direction, see Eq. 1, and d_0 the distance defined by Eq. 2.

$$\omega'^2 = \omega^2 + (d_0 - d)^2 \quad (1)$$

$$\text{with: } d_0^2 = (R_1 + R_2)^2 - \omega^2 \quad (2)$$

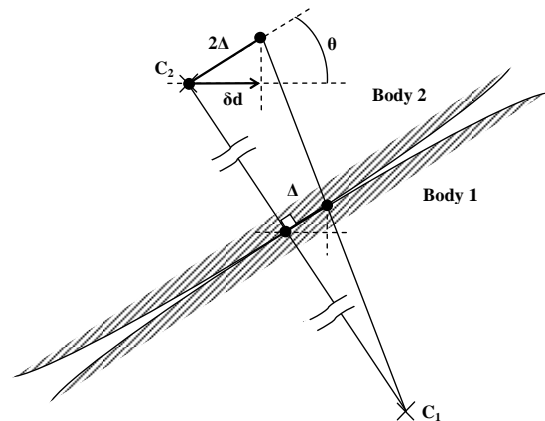


Fig. 6 – Displacement δd of body 2

In this formulation, the fixed value is the shifting value Δ introduced in Fig. 2. As a consequence, it is required to express the sliding distance d as a function of Δ . At any time, if one of the bodies is displaced from a value δd , its surface makes an angle θ with the shifting direction, see Fig. 6. It is then possible to write:

$$\delta d = 2\Delta \cdot \cos \theta \quad (3)$$

Considering the curvature of the bodies, a correction has to be made to the value δd . Denoting $\widehat{\Delta}$ the real shifted value, see Fig. 7, and writing that:

$$\tan \alpha = \frac{\Delta}{\omega_{i-1}'/2} \quad (4)$$

ω_{i-1}' being the previous local separation, δd can be corrected as follows:

$$\delta d = 2\widehat{\Delta} \cdot \cos \theta \quad (5)$$

$$\text{with: } \widehat{\Delta} = (\omega_{i-1}'/2) \cdot \alpha = (\omega_{i-1}'/2) \cdot \tan^{-1}\left(\frac{\Delta}{\omega_{i-1}'/2}\right) \quad (6)$$

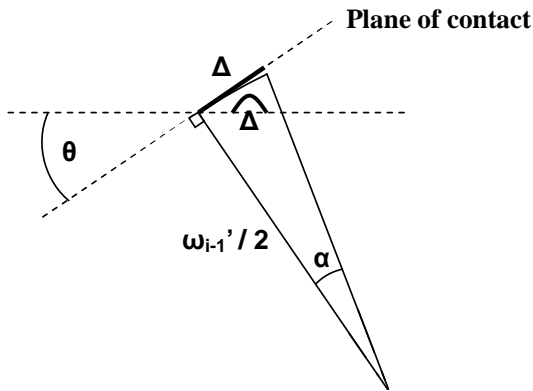


Fig. 7 – Correction of the term δd

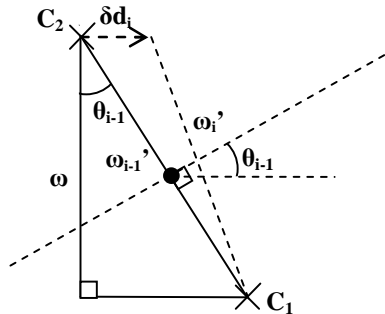


Fig. 8 – Representation of two consecutive states $i-1$ and i for the determination of θ_{i-1}

Then δd can be re-written as follows:

$$\delta d_{i-1} = \omega_{i-1}' \cdot \tan^{-1}\left(\frac{\Delta}{\omega_{i-1}'/2}\right) \cdot \cos \theta_{i-1} \quad (7)$$

Now θ is determined, which is an unknown and varies with the sliding distance. Considering two consecutive states $i-1$ and i , see Fig. 8, one can write:

$$\cos \theta_{i-1} = \frac{\omega}{\omega_{i-1}'} \quad (8)$$

Coupling Eqs. 7 and 8, it yields:

$$\delta d_i = \omega \cdot \tan^{-1}\left(\frac{2\Delta}{\omega_{i-1}'}\right) \quad (9)$$

The last step in the determination of the sliding distance d is the summation of all the sliding distance increments, i.e.:

$$d_i = \sum_{k=1}^i \delta d_k \quad (10)$$

i being the current state. The explicit form of d_i is then:

$$d_i = \omega \cdot \sum_{k=0}^{i-1} \tan^{-1}\left(\frac{2\Delta}{\omega_k'}\right) \quad (11)$$

Finally, combining Eqs. 1, 2 and 11, the local separation can be re-written as follows, at every step of the computation:

$$\omega_0' = (R_1 + R_2) \quad (12)$$

$$i > 0: \omega_i' = \left[\omega^2 + \left[\left[(R_1 + R_2)^2 - \omega^2 \right]^{1/2} - \omega \cdot \sum_{k=0}^{i-1} \tan^{-1}\left(\frac{2 \cdot \Delta}{\omega_k'}\right) \right]^2 \right]^{1/2} \quad (13)$$

In order to relate the local center separation ω' to the interference (rigid body approach) α used in the Semi-Analytical Code developed previously, one can write:

$$\alpha_i = (R_1 + R_2) - \omega_i' \quad (14)$$

Force calculation and results

The first part of this section deals with the force calculation that is projected in the global reference. Some correction term will be added in order to take into consideration what the authors refer as “pile-up” phenomenon. Finally, some results will be plotted concerning the tangential and normal forces found during the sliding phase, as well as the energy loss in the sliding contact, and the residual deformation after unloading at the end of the sliding process.

Force calculation in the global reference

At anytime during sliding, it is possible to calculate the pressure distribution resulting from the normal contact in the local reference. As a consequence, the tangential and the normal forces in the global reference can be calculated by integrating the pressures on the X and Y axes for the tangential forces, and on the Z-axis for the normal force, i.e.:

$$F_X = n \cdot a_x \cdot a_y \cdot \sum_{I_c} p \cdot \sin \theta \quad (15)$$

$$F_Y = n \cdot a_x \cdot a_y \cdot \sum_{I_c} p \quad (16)$$

$$F_Z = n \cdot a_x \cdot a_y \cdot \sum_{I_c} p \cdot \cos \theta \quad (17)$$

n being the number of nodes where the contact pressure is not nil, a_x and a_y the grid spacing in x' and y' direction respectively (local reference), and I_c the set of nodes where the pressure is not nil. As an example, Fig. 9 shows how to obtain the projected forces at a point of the contact surface. Due to the symmetry of the problem, the projected force F_Y on the Y-axis is nil.

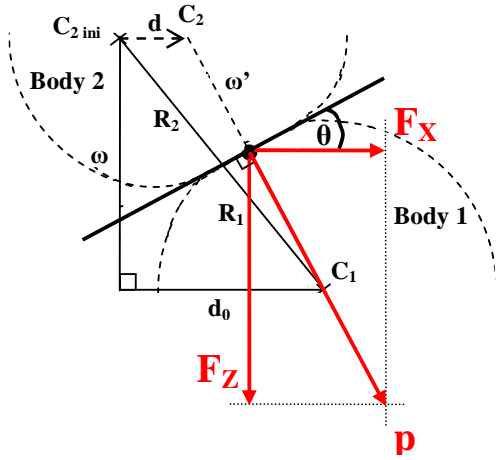


Fig. 9 – Projection in the global reference of the force at a point of the contact surface

Correction term induced by the “pile-up”

The previous force calculation only takes into account the macro-scale projection. In order to include the effect of the pile-up, it is necessary to study the micro-scale projection. Fig. 10 shows a magnified view at the point where the pressure p is applied. The residual displacement u^r has a slope that makes an angle θ_{px} with the x' -axis and θ_{py} with the y' -axis.

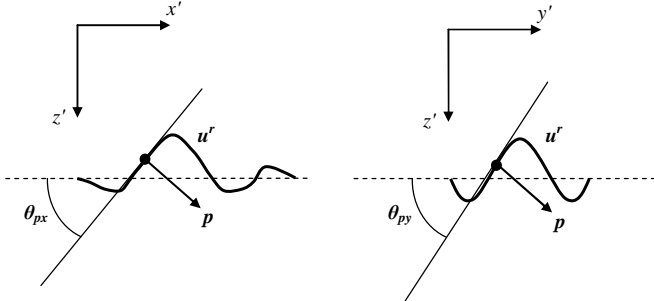


Fig. 10 – Effect of the pile-up due to the slope of the residual displacement

From this observation, Eqs. 15, 16, and 17 can be corrected as follows:

$$F_X = n \cdot a_x \cdot a_y \cdot \sum_{I_c} p \cdot \sin(\theta - \theta_{px}) \quad (18)$$

$$F_Y = n \cdot a_x \cdot a_y \cdot \sum_{I_c} p \cdot \sin(-\theta_{py}) \quad (19)$$

$$F_Z = n \cdot a_x \cdot a_y \cdot \sum_{I_c} p \cdot \cos(\theta - \theta_{px}) \cdot \cos(\theta_{py}) \quad (20)$$

$$\text{with: } \theta_{px} = \tan^{-1} \left(\frac{\partial u^r}{\partial x} \right) \quad (21)$$

$$\text{and } \theta_{py} = \tan^{-1} \left(\frac{\partial u^r}{\partial y} \right) \quad (22)$$

From Eq. 8, θ can be expressed as:

$$\theta = \cos^{-1} \left(\frac{\omega}{\omega_i} \right) \cdot \text{sign}(\omega_i - \omega_{i-1}) \quad (23)$$

Results

The next simulations have been inspired from the work of Vijaywargiya and Green [15] who modeled the sliding contact between two cylinders using a Finite Element model. For the current simulations, two spherical asperities will interact. The radius of the spheres can be taken arbitrarily, so $R_1 = R_2 = 1$ m has been chosen. The elastic properties are $E_1 = E_2 = 200$ GPa for the young moduli, and $\nu_1 = \nu_2 = 0.32$ for the Poisson ratios. The chosen hardening law holds for perfect plasticity with parameter $S_y = 0.9115$ GPa for the yield stress.

In most of the results presented, values are normalized by the critical values defined by Green in [21] corresponding to the onset of yielding when plasticity just starts occurring:

$$\alpha_c = \left(\frac{\pi C S_y}{2 E'} \right)^2 R \quad (24)$$

$$P_c = \frac{(\pi C S_y)^3 R^2}{6 E'^2} \quad (25)$$

$$U_c = \frac{(\pi C S_y)^5 R^3}{60 E'^4} \quad (26)$$

with α_c the critical interference, P_c the critical load and U_c the maximum potential energy stored during elastic deformation, equals to the work done. In these equations, parameter C is expressed in function of Poisson ratio [21]:

$$C(\nu) = 1.30075 + 0.87825 \nu + 0.54373 \nu^2 \quad (27)$$

Hereafter are plotted the reaction forces during the first sliding pass. The forces are normalized by the critical force found in Eq. 25, here $P_c = 3.461 \cdot 10^5$ N, and the abscissa along the sliding direction by the equivalent radius in Eq. [28] i.e. $R=0.5$ m. Figures 11 and 12 give the tangential and the normal forces, respectively.

$$\frac{1}{R} = \frac{1}{R_1} + \frac{1}{R_2} \quad (28)$$

It can be seen in Fig. 11 that for small interference values, the tangential force is anti-symmetric, and vanishes when the asperities are perfectly aligned, i.e. for $X/R = 0$. On the other hand, for large values of the interference, one can see that the curve is not anti-symmetric anymore. It means that most of the energy (area under the curve) is produced during loading, i.e. before the asperities are aligned, and just a small part of the energy is released during unloading, i.e. when the asperities are repulsing each other. Also, the value of the force when the asperities are aligned does not vanish anymore; this phenomenon is due to plastic deformation. Indeed, the residual displacement on the surface of the bodies induces some pile-up

since the normal contact plane is not parallel to the sliding direction any longer.

The normal force plotted in Fig. 12 is symmetric for low interference values. Then a slight asymmetry begins to appear when increasing the interference, however less pronounced than for the tangential force. Again, this phenomenon is due to plasticity, since due to the permanent deformation of the surface that take place during the first loading cycle the normal contact plane and the sliding direction are not parallel.

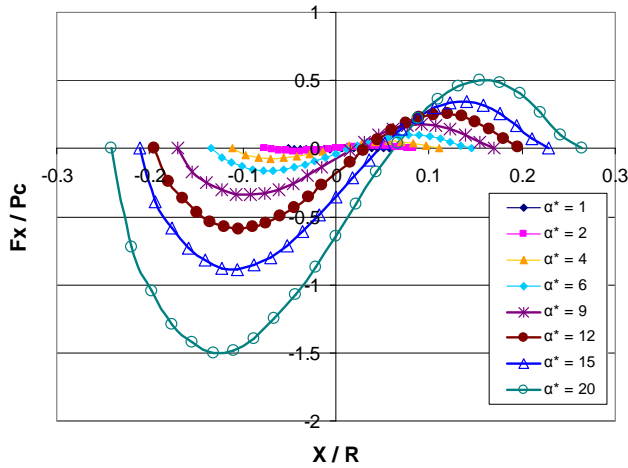


Fig. 11 – Dimensionless tangential force during sliding vs. dimensionless sliding direction

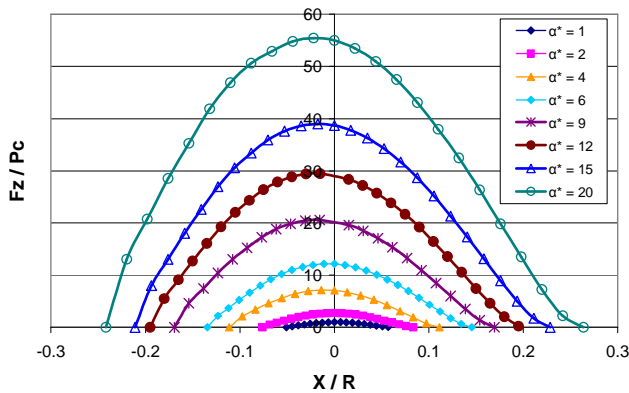


Fig. 12 – Dimensionless normal force during sliding vs. dimensionless sliding direction

To give an idea of energy loss during the sliding process, figure 13 shows the evolution of the net energy normalized by the critical energy found in Eq. 26, versus the dimensionless interference.

A load ratio is now defined as F_x / F_z the ratio of the tangential force over the normal one. Results are plotted in Fig. 14 versus the normalized sliding distance. It should be noted that the current simulation was made under the assumption of frictionless contact, therefore the load ratio is only related here to the ploughing or tugging phenomena. It can be seen that for small interference values this ratio is almost perfectly

antisymmetric. An increase of the load ratio is found at the beginning of the tugging (left part of Fig. 14) when increasing the interference. Conversely the F_x / F_z ratio tends to reach an asymptotic value of 0.045 at the end of the contact (right part of the curves). In addition, it can be observed that this ratio is not nil anymore when the asperities are aligned, this offset increasing with the interference value. It is again assumed to be due to plastic deformation inducing pile-up.

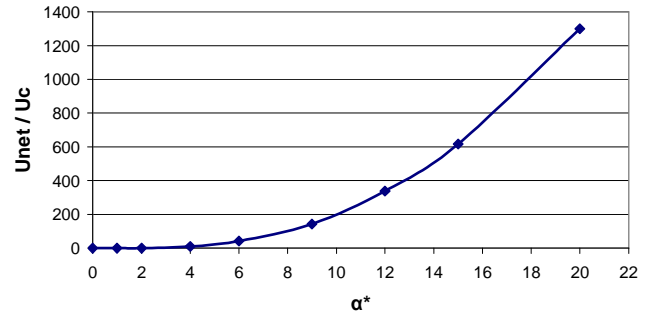


Fig. 13 – Dimensionless net energy vs. dimensionless interference

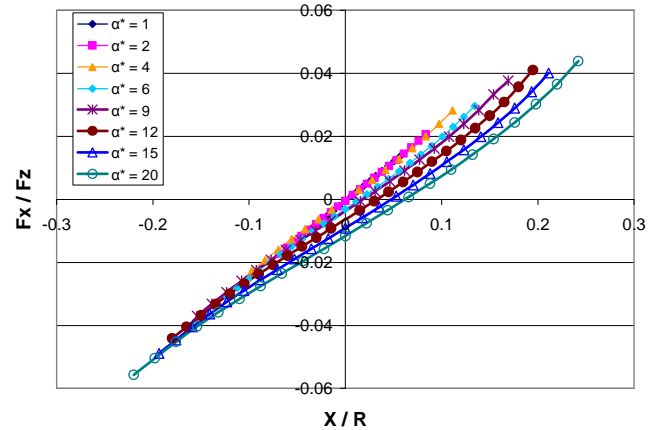


Fig. 14 – Load ratio during sliding vs. dimensionless sliding direction

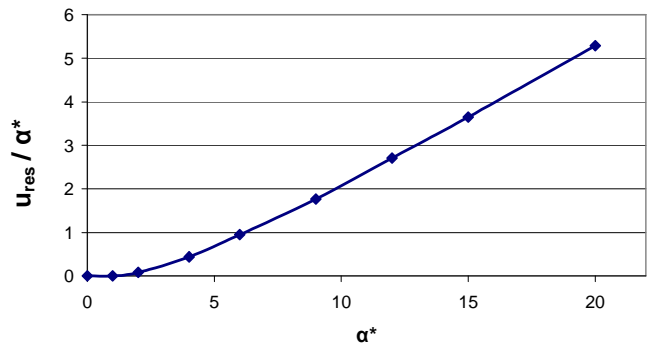


Fig. 15 – Dimensionless residual displacement vs. dimensionless interference

Another interesting result is the evolution of the permanent deformation of the surface. Figure 15 shows the maximum value of the residual displacement after unloading normalized by the critical interference given in Eq. 24, as a function of the interference. It shows a very significant residual deformation of the surface, up to 25% of the interference.

Representative computation times corresponding to $\alpha^* = 9$, for the mesh-size $dx=3.85\text{mm}$, $dy=7.7\text{mm}$, $dz=1.925\text{mm}$ (i.e., $33 \times 13 \times 31 = 13,299$ points) in the plastic zone, and 25 time-step increments to describe the relative motion, took about 25 minutes on a 1.8 GHz Pentium M personal computer.

CONCLUSION

A novel way of modeling an elastic-plastic rolling / sliding contact has been presented. For that purpose a tri-dimensional thermal-elastic-plastic code has been adapted in a companion paper [13]. Two formulations have been proposed to drive the computation, one by imposing the load and the second one by imposing a normal rigid body displacement also call contact interference. The tugging between two single asperities has then been investigated. Results have shown that plasticity produces an asymmetry of the normal and tangential loading during the transient contact. A load ratio due to ploughing has been estimated.

Compared to Finite Element modeling, the developed code allows the user to compute a rolling and sliding contact in very short CPU times. The current work provides the foundation to incorporate thermal-electrical-mechanical interaction between rough surfaces by progressively introducing the relevant physical phenomena.

REFERENCES

- [1] Jacq, C., Nélias, D., Lormand, G., and Girodin, D., 2002, "Development of a Three-Dimensional Semi-Analytical Elastic-Plastic Contact Code," *ASME J. Tribol.*, **124**, pp. 653–667.
- [2] Liu, S., Wang, Q., 2001, "A Three-Dimensional Thermomechanical Model of Contact Between Non-Conforming Rough Surfaces," *ASME J. Tribol.*, **123**, pp. 17–26.
- [3] Boucly, V., Nélias, D., Liu, S., Wang, Q. J., and Keer, L. M., 2005, "Contact Analyses for Bodies With Frictional Heating and Plastic Behavior," *ASME J. Tribol.*, **127**, pp. 355–364.
- [4] Nogi, T., and Kato, T., 1997, "Influence of a Hard Surface Layer on the Limit of Elastic Contact—Part I: Analysis Using a Real Surface Model," *ASME J. Tribol.*, **119**, pp. 493–500.
- [5] Polonsky, I. A., and Keer, L. M., 1999, "A Numerical Method for Solving Rough Contact Problems Based on the Multi-Level Multi-Summation and Conjugate Gradient Techniques," *Wear*, **231**, pp. 206–219.
- [6] Lubrecht, A. A., and Ioannides, E., 1991, "A Fast Solution of the Dry Contact Problem and the Associated Sub-Surface Stress Field, Using Multilevel Techniques," *ASME J. Tribol.*, **113**, pp. 128–133.
- [7] Liu, S., Wang, Q., and Liu, G., 2000, "A Versatile Method of Discrete Convolution and FFT (DC-FFT) for Contact Analyses," *Wear*, **243**, pp. 101–111.
- [8] Jacq, C., Lormand, G., Nélias, D., Girodin, D., and Vincent, A., 2003, "On the Influence of Residual Stresses in Determining the Micro-Yield Stress Profile in a Nitrided Steel by Nano-Indentation," *Materials Science and Engineering A*, **342**, pp.311-319.
- [9] Sainsot, P., Jacq, C., and Nélias, D., 2002, "A Numerical Model for Elastoplastic Rough Contact," *Computer Modeling in Engineering & Sciences*, **3** (4), pp.497-506.
- [10] Nélias, D., Antaluca, E., Boucly, V., and Cretu, S., 2006, "A 3D Semi-Analytical Model for Elastic-Plastic Sliding Contacts," submitted.
- [11] Gallego, L., Nélias, D., and Jacq C., 2006, "A Comprehensive Method to Predict Wear and to Define the Optimum Geometry of Fretting Surfaces," *ASME J. Tribol.*, **128**, pp.476-485.
- [12] Nélias, D., Boucly, V., and Brunet, M., 2006, "Elastic-Plastic Contact Between Rough Surfaces: Proposal for a Wear or Running-in Model," *ASME J. Tribol.*, **128**, pp. 236–244.
- [13] Boucly, V., Nélias, D., and Green, I., 2006, "Modeling of the Rolling and Sliding Contact Between two Asperities. Part I: Numerical Methodology," *Proc. of IJTC2006, STLE-ASME Int. Joint Trib. Conf.*, October 22-25, 2006, San Antonio, TX, USA, Paper IJTC2006-12103.
- [14] Chen, J., Akyuz, U., Xu, L., and Pidaparti, R. M. V., 1998, "Stress Analysis of the Human Temporomandibular Joint," *Medical Engineering & Physics*, **20**(8), pp. 565-572.
- [15] Vijaywargiya, R., Green, I., 2006, "A Finite Element Study of the Deformation, Forces, Stress Formation, and Energy Loss in Sliding Cylindrical Contacts," *Proc. of IJTC2006, STLE-ASME Int. Joint Trib. Conf.*, October 22-25, 2006, San Antonio, TX, USA, Paper IJTC2006-12020.
- [16] Hamilton, G. M., Goodman, L.E., 1966, "The Stress Field Created by a Circular Sliding Contact," *ASME J. Appl. Mech.*, **33**, pp. 371-376.
- [17] Hamilton, G. M., 1983, "Explicit Equations for the Stresses Beneath a Sliding Spherical Contact," *Proceedings of the Institution of Mechanical Engineers, Part C (Mechanical Engineering Science)*, **197**, p. 53-59.
- [18] Kogut, L., Etsion, I., 2003, "A Semi-Analytical Solution for Sliding Inception of a Spherical Contact," *ASME J. Tribol.*, **125**(3), pp. 99-506.
- [19] Faulkner, A., Arnell, R. D., 2000, "Development of a Finite Element Model to Simulate the Sliding Interaction Between two, Three-Dimensional, Elastoplastic, Hemispherical Asperities," *Wear*, **242**(1), p. 114-122.
- [20] Nosonovsky, M., Adams, G. G., 2000, "Steady-State Frictional Sliding of two Elastic Bodies with a Wavy Contact Interface," *ASME J. Tribol.*, **122**(3), pp. 490-495.
- [21] Green, I., 2005, "Poisson Ratio Effects and Critical Values in Spherical and Cylindrical Hertzian Contacts," *Int. J. Appl. Mech. and Eng.*, **10**(3), pp. 451-462.